In-situ tin casting combined with three-dimensional scanner to quantify structural characteristics of anecic earthworm burrows

Na Wen [a], Jie Zhang [a], Hui Zeng [a], Gang Liu [a*], Robert Horton [b]

[a] Department of Land Use Engineering, College of Land Science and Technology, China Agricultural University, Beijing 100193, China.

[b] Department of Agronomy, Iowa State University, Ames, IA 50011, USA.

This work was supported by Natural Science Foundation of China (Grant No 42077008 and Grant No 41771257), and USDA-NIFA Multi-State Project 4188.

[*] Corresponding author (Email: liug@cau.edu.cn)

Email: wenna1422@163.com (Wen Na)

Core Ideas

- Tin casting can be used for in situ extraction of anecic earthworm burrows open at the soil surface.
- Tin casting and 3D laser scanning can successfully digitize the spatial characteristics of earthworm burrows.
- There are no statistical differences in the tortuosity of burrows at two different sites.

Abstract

Earthworms play a critical role in soil ecosystems. Analyzing the spatial structure of earthworm burrows is important to understand their impact on water flow and solute transport. Existing in-situ extraction methods for earthworm burrows are time-consuming, labor-intensive and inaccurate, while CT scanning imaging is complex and expensive. The aim of this study was to quantitatively characterize structural characteristics (cross-sectional area (A), circularity (C), diameter (D), actual length (L_t), tortuosity (τ)) of anecic earthworm burrows that were open and connected at the soil surface at two sites of different tillage treatments (no-till at Lu Yuan (LY) and rotary tillage at Shang Zhuang (SZ)) by combining a new in-situ tin casting method with three-dimensional (3D) laser scanning technology. The cross-sections of anecic earthworm burrows were almost circular, and the C values were significantly negatively correlated with D and A. Statistically, there were no significant differences in the τ values (1.143 ± 0.082 vs 1.133 ± 0.108) of anecic earthworm burrows at LY and SZ, but D (6.456 ± 1.585 mm) and A (36.929 ± 21.656 mm^2) of anecic earthworm burrows at LY were significantly larger than D (3.449 ± 0.531 mm) and A (9.786 ± 2.885 mm^2) at SZ. Our study showed that burrow structures at two different sites differed from each other. Soil tillage methods, soil texture and soil organic matter content at the two sites could have impacted earthworm species composition, variation of earthworm size and the morphology of burrows. The method used in this research enabled us to adequately assess the spatial structure of anecic earthworm burrows in the field with a

Abbreviations: A, cross-sectional area; CT, X-ray computed tomography; C, circularity; D, diameter; 3D, three-dimensional; LY, Lu Yuan; L_1, vertical length; L_t, actual length; P, section perimeter; SZ, Shang Zhuang; τ, tortuosity.

limited budget.

Key Words: Anecic earthworm burrow; Tin casting; Three-dimensional (3D) laser scanner; Tortuosity; Macropore

1 INTRODUCTION

Earthworms play a key role in the ecology of soils in many regions of the world (Gavinelli et al., 2018). Burrows formed through earthworm activity behave as preferential pathways, which can have an important impact on the conversion, storage, and utilization of precipitation and the migration of pollutants in the soil. Existing studies (Bastardie, Capowiez, de Dreuzy & Cluzeau, 2003; Perret, Prasher, Kantzas & Langford, 2000; Peth et al., 2008) have demonstrated that the infiltration rate of soil water and solute associated with particular burrow systems relies heavily on the three-dimensional (3D) spatial properties, namely, pore diameter (D), cross-sectional area (A), circularity (C), actual length (L_t) and tortuosity (τ). Therefore, accurate measurement and quantification of 3D structural characteristics of earthworm burrows is very important for hydrological modeling, especially the transport of water and solute in soil with earthworm burrows. However, the exact spatial structure of earthworm burrows is still poorly understood and studied. At present, popularly used hydrological and soil physical process software lacks quantitative parameters of earthworm burrow structure (Le Mer et al., 2021). For example, Hydrus (Šimůnek, van Genuchten & Šejna, 2008), Feflow (Peleg & Gvirtzman, 2010) and WHCNS (Liang, Hu, Batchelor, Qi & Li, 2016) considered only macroporosity other than structure parameters (D, A, C, L_t, τ) for studying macropores. However, in order to accurately model the effects of macropores such as earthworm burrows on water and solute transport, these

spatial parameters need to be taken into account. Currently, methods for extracting macropore spatial parameters include in situ extraction methods, as well as non-contact extraction methods.

For the extraction of in situ earthworm burrow morphology, the major methods include the following: liquid latex and resin infusion (Li et al., 2019; Li, Shao, Jia, Jia & Huang, 2018), and dye tracing (Filipović et al., 2020). However, each method has limitations, and none are used widely. (1) The solidification process of castings formed with liquid latex, resin and gypsum slurry usually takes 8-12 h (Abou Najm, Jabro, Iversen, Mohtar & Evans, 2010), which is time-consuming. And the volume shrinkage of resin castings is 6-7 % after fully cured (Nawab, Boyard, Sobotka, Casari & Jacquemin, 2011). (2) Castings formed through these materials are prone to deform and fracture during the extraction process and are not suitable for transportation and preservation. (3) Resins have been used to prepare soil thin sections for decades, however, the diffusion of resin within soil matrix micropores makes the solidified resin casts difficult to separate from soil, plant debris and other debris (Tippkoetter & Ritz, 1996). (4) Compared with metal tin, the low density of resin (typically less than 1.2 g/cm^3), latex and gypsum slurry, as well as their large dynamic viscosity values (Reis, 2012) are related to penetration resistance for infiltrating deeply into soil, which results in incomplete castings and large measurement errors. To overcome the disadvantages of traditional filling materials (resin, latex and gypsum slurries), the smaller volume shrinkage (about 3 % versus 6-7 % for resins) and denser metal tin (7.3 g/cm^3 versus about 1.2 g/cm^3 for resins) (Gancarz, Moser, Gąsior, Pstruś & Henein, 2011) with dynamic viscosity less than 1‰ the value of resin, was chosen to cast earthworm burrows. So far, no studies on the use of metal tin for earthworm

burrow morphology extraction have been reported.

Dye tracer is another method that have been used to monitor water flow within soil profile and to estimate the size and distribution of soil pore (Zhang et al., 2019; Zhang, Lei & Chen, 2016), but dye staining have difficulties in practical applications. Germán-Heins and Flury (2000) showed that adsorption of dyes in soils was affected by soil pH, ionic strength, and soil composition, and thus was prone to large errors. Filipović et al. (2020) suggested that the adsorption of dyes on pore walls led to overestimation of flow. Kodešová et al. (2015) confirmed that dye distribution was significantly affected by the presence of large pores, root system, and organic matter in the soil, resulting in the inability to quantify the spatial distribution of macropores.

Thus, to overcome the drawbacks of the above mentioned methods for in situ extraction of macropores, non-contact and non-invasive methods represented by X-ray computed tomography (CT) are often used when precision is the major focus of soil pore study (Cercioglu, 2018). For example, Borges et al. (2019) and Luo, Lin and Li (2010) quantified the structure of 3D morphological features of soil macropores by applying CT techniques. However, CT imaging methods still have many challenges for analyzing the 3D characteristics of in situ soil macropores, including: (1) Due to the large size and operation limitations of CT machines, it is almost impossible to perform in situ analysis in the field. (2) CT scanning technology has limits on the size of the sample, which is generally less than 20 cm (Capowiez, Bottinelli, Sammartino, Michel & Jouquet, 2015), making it difficult to use this method for extracting burrow morphology of anecic earthworms. (3) 3D images created by CT equipment must be opened

and processed with specific software or programs (Kuzminsky & Gardiner, 2012). During CT image processing, the accuracy will be influenced by thresholds used to separate soil pores from soil particles and the segmentation algorithms (Iassonov, Gebrenegus & Tuller, 2009; Taina, Heck & Elliot, 2008). (4) Due to the cost of CT equipment, this method is expensive and not suitable for extracting earthworm burrow morphology in large quantities in the field (Pagenkemper et al., 2015). (5) Field-collected soil samples need to prevent soil shrinkage due to water evaporation (Gebrenegus, Ghezzehei & Tuller, 2011) and avoid dry crack formation (Krisnanto, Rahardjo, Fredlund & Leong, 2016). The soil samples can be easily distorted by compression when field-collected in-situ soil samples are excavated for CT experiments, which leads to distortion of macropores and deviates from the original geometry (Hanna, Steward & Aldinger, 2010). In addition, this method cannot effectively distinguish between plant root pores and worm pores (Mooney, 2002). These factors lead to unavoidable errors when extracting structural features of earthworm burrows using CT imaging methods.

3D laser scanning technology can collect 3D coordinate information of large, complex, and irregular objects. Based on the collected 3D cloud data, not only can the spatial structure of scanned objects be reconstructed, but also a series of post-processing analyses, quantitative analysis of the obtained digital burrow morphology structure, e.g., can be accomplished. In addition, with the rapid development of numerical simulation software (COMSOL and ANSYS) (Ni, Miao, Lv & Lin, 2017; Zhang et al., 2017), 3D point cloud data can be converted into the specific file formats required to use the simulation software, thereby generating 3D geometry meshes for numerical simulations. Since the 3D laser scanning method is non-destructive, the

scanned geometry can also be used for other analyses (Rossi, Hirmas, Graham & Sternberg, 2008), such as pore connectivity and pore size distribution. But we are not aware of studies using 3D laser scanners for morphological characterization of macropores in the field.

The combination of recently developed 3D laser scanners and in-situ extraction of pore structure can overcome most of the above mentioned limitations of CT methods (the size of the sample to be measured is smaller than the length of a typical earthworm burrow, and soil structure can be damaged when the sample is collected). In addition, the newly proposed method does not need complex segmentation algorithms unlike CT scanned images. Currently, 3D laser scanners have been widely used in archaeological excavations and restoration of cultural objects due to their high spatial resolution (5 μm), simplicity of operation, and low experimental error (Kuzminsky & Gardiner, 2012).

This research explores a new method to quantitatively characterize anecic earthworm burrows that are open at the soil surface. The objectives of this study are to examine the feasibility of infusing metal tin into in situ continuous earthworm burrows open at the soil surface to obtain three-dimensional structural castings of the burrow, to digitize the spatial structure of earthworm burrow castings with a 3D laser scanner, and to obtain parameters such as cross-sectional area (A), circularity (C), diameter (D), actual length (L_t) and tortuosity (τ). Based on the earthworm burrow spatial parameters (A, C, D, L_t, τ), the differences in earthworm burrow morphology and the factors affecting these parameters are analyzed and compared for two different test sites.

2 MATERIALS AND METHODS

2.1 Study site

The field experiments were performed at the Lu Yuan (LY) experimental site and the Shang Zhuang (SZ) experimental site of China Agricultural University, Hai Dian District, Beijing (Figure 1), which are in the alluvial plains area of the North China Plain. The two test sites are approximately 15 km apart from each other. The climate type is temperate humid monsoon climate zone with a mean annual precipitation of 534 mm, of which ≥ 70 % occurs between July and September. The average annual temperature is 13.2 °C. According to the USDA soil taxonomy system, soil in LY was silt loam, and the soil organic matter content was 10.5 $g \cdot kg^{-1}$; soil in SZ was sandy loam, and the soil organic matter content was 6.4 $g \cdot kg^{-1}$. The test sites had rain-fed agricultural systems. LY was traditional farmland that had been continuously no-till for 13 years (since year 2009). The main crops grown were spring maize and autumn cabbage without mulch all year round. The SZ site was on a long-term locational experiment station under traditional rotary tillage since 2005. Sweet potatoes were grown all year round without mulch and were manually tilled once a year before planting. No crops were planted and no farm management practices were carried out in the two sites during the earthworm burrow measurement period.

2.2 Experiment design

We randomly selected study areas with dimensions of 4 m × 5 m at the two field sites (Figure 2a). Each area was divided into 20 square plots of 1 m × 1 m by a plastic tubing placed on soil surface (Figure 2b). We placed flags to mark where earthworm feces were accumulated on the ground surface (Figure 2c), and removed the weeds and debris at the entrance of the

burrows. The density of earthworm burrows that were open at the soil surface was calculated by counting the number of flags in experimental sites. Then, adult earthworms were collected by electric shock method to obtain information on population density and species level (Pelosi, Baudry & Schmidt, 2021).We pushed two electrode rods (made of stainless steel, 420 mm long, 4 mm in diameter, horizontal spacing of 50 cm) of the electric shock apparatus into the soil to a depth of 42 cm within the 1 m^2 square area enclosed by plastic tubing. The two rods of the electric shocking machine were connected to a 12 V battery. Current was passed through the soil volume surrounding the two rods. Approximately 5 minutes after applying the electric shock, the shocked earthworms escaped to the soil surface. Emerging earthworms were collected in sterile centrifuge tubes. The earthworms no longer emerged out of the ground after about 35 minutes. The population density of earthworms was determined by counting the number of adult earthworms (identified by the presence of clitellum formation) (Takacs et al., 2016) at each sampling location. Earthworm samples from the two sites were respectively fixed and stored in 95% ethanol for transport back to the laboratory.

After collecting the earthworms, metal tin was used to fill the earthworm burrows to make the castings. Metal tin held in a pot was heated with a field windproof portable butane stove to temperatures of 250-300 °C, exceeding the melting point of the metal tin (232 °C) (Alavi & Passandideh-Fard, 2011). An infrared thermometer was used to monitor the tin temperature, so as not to overheat the tin. Melted tin was poured slowly and continuously into the earthworm burrows at their surface openings, to ensure that tin infiltrated into deeper and smaller pores. We carefully excavated castings from the soil by using a shovel, cleaned all remaining soil

particles adhering to the surface of castings and then took photos of the castings (Figure 2d). The melting of metal tin usually took 20-30 min and the entire solidified process of tin castings usually took only 8-12 s. Unlike resin, latex and gypsum, the formed tin castings were not only resistant to deformation and could be conveniently stored for further analysis, but the tin did not adhere to soil, which enabled the extracted castings to accurately reflect the spatial structure of the burrows. In addition, the relatively dense tin easily infiltrated into the deep soil and made the extracted burrow castings complete and reliable. However, one shortcoming of tin casting is that the method is not suitable for use in saturated or nearly saturated soil. The melted tin can quickly vaporize moisture within burrows, and the escaping water vapor can cause the tin to splash out. So, face shielding and gloves should be worn to protect from skin burns.

The ABI 3730XL automatic capillary sequencer (Applied Biosystems, Foster City, CA, USA) was used to sequence earthworm genes, and the sequencing primers were the same as the PCR primers. The sequencing results were submitted to the National Center for Biotechnology Information (NCBI) database, and a sequence similarity search was performed in the GenBank database by BLAST (Basic Local Alignment Search Tool) to ensure the accuracy and reliability of sequencing results.

2.3 3D laser scanner

A Tian Yuan blue light three-dimensional scanner OKIO-5M (Tian Yuan 3D Technology Limited company, Beijing, China) was used to collect data points on the structure of the 3D burrow castings. The system consists of an industrial camera with a resolution of 5 million pixels. The measurement accuracy is 0.01 mm, and the spatial resolution is 5 μm. An illustration

of the 3D scanner is shown in Figure 3.

2.4 Structural parameters

After reconstructing the spatial structure of the earthworm burrows, structural parameters were analyzed quantitatively with the help of Geomagic Design X (2019 version) and Image J software (Li, Shao, Jia, Jia & Huang, 2018). The A and section perimeter (P) of earthworm burrows were directly calculated by using Geomagic Design X software. The C for earthworm burrows was defined as follows (Capowiez, Bottinelli, Sammartino, Michel & Jouquet, 2015; Capowiez, Sammartino & Michel, 2011; Pagenkemper et al., 2015)：

$$C = 4\pi A / p^2 \quad (1)$$

Assuming that the shape of all macropores was cylindrical, its D was calculated as (Capowiez, Sammartino & Michel, 2011):

$$D = 2\sqrt{A/\pi} \quad (2)$$

The τ (Luo, Lin & Li, 2010) was calculated as the ratio of the actual length of the earthworm burrow (L_t) to the vertical length (L_1) (Figure 4):

$$\tau = L_t / L_1 \quad (3)$$

2.5 Data analysis

Analysis of variance and correlation analyses were performed by using SPSS (version 24.0, SPSS Inc., Chicago, IL). The comparisons of the characteristic parameters of anecic earthworm burrows were performed by using one-way ANOVA. Origin 8.0 software (Origin Lab, Northampton, ME) and Photoshop CS6.0 (Adobe Systems Corporation, San Jose, US) were used to create the figures.

3 RESULTS AND DISCUSSION

3.1 Species and density of earthworms

In this research, 20 adult earthworms were selected from both LY and SZ, respectively for gene sequencing. The sequencing results (Table 1) show that all successfully sequenced samples (30 earthworms) belonged to Megascolecidae. All earthworms at LY were Metaphire vulgaris. SZ had two genera and three species, that was, Amynthas amis, Metaphire vulgaris and Metaphire tschiliensis tschiliensis, respectively. Among them, Amynthas amis accounted for 60 % of the total number of earthworms in SZ. By in-situ observing the shape of earthworms, the burrows spatial characteristics, as well as activity range of earthworms in the field, we found that all earthworms in the above two study areas were anecic. The average body length of earthworms in LY was 140 mm and the average body diameter was 6 mm, while the average body length of earthworms in SZ was 106 mm and the average body diameter was 3 mm.

Table 2 shows that, the densities of anecic earthworm burrows that were open at the soil surface at LY and SZ were 2.7 (burrows / m^2) and 1.4 (burrows / m^2) respectively, and the population densities of anecic earthworms were 16.1 (individuals / m^2) and 4.2 (individuals / m^2), respectively. The reasons why the density of anecic earthworm burrows was much lower than the population density of anecic earthworm might be that some earthworm burrows collapsed due to rainfall, tillage treatment, and human disturbance. All these factors resulted in the blockage of the burrows, and thus underestimation of burrow density. Chan (2001) found that the number of earthworms per square meter under conservation tillage was 2-9 times that of earthworms in conventional tillage. Our results were consistent with the findings of Chan

(2001). The no-till (LY) field had high soil organic matter content, which could provide substantial food and energy for earthworms. Rotary tillage (SZ) disturbed burrows which might have caused a significant reduction in the earthworm population through mechanical damage to burrows (Peigne et al., 2009). Finally, soil texture differences between the two sites resulted in different tunneling resistance and burrow strength. The more compacted sandy loam at SZ was harder for earthworms to dig than the soil at LY.

3.2 Visualization of earthworm burrows

Most of the extracted earthworm burrows were less than 150 mm in length (Figure 5), which was the result of the following factors for casting tin in the field. The presence of earthworms, earthworm feces and soil aggregate particles in the burrow caused the burrows at certain depth were partially filled or blocked, resulting in the castings at these locations to more likely be broken. Occasionally, we had earthworms and soil aggregate contained within the tin casting. As a result, many samples up to 400-500 mm in length were broken during handling and excavation, because of the fragile parts. Under these conditions, we selected a relatively intact section to digitalize the morphological features of the burrow cast. In a future study, we will consider how to improve this method to extract more complete and longer casts of earthworm burrows. For example, by applying multiple electric shocks before casting, to ensure that no earthworms are present in the burrow. To clean up debris clogging the burrow as much as possible by vacuuming those burrows before casting tin.

Figure 5 shows the spatial structure, determined by the 3D scanner and the metal-tin casts, of digitized earthworm burrows at two field sites, LY and SZ. Although tillage was different at

the two sites, some burrow structure characteristics were similar. For example, earthworm burrows were mainly cylindrical in shape, with a general trend of vertical downward and only a few branches extending laterally, which might be related to the fact that we extracted anecic earthworm burrows. In addition, the high spatial resolution of the 3D scanner (5 μm) captured the uneven spatial features of the burrow surfaces. The *D* values of earthworm burrows at LY were significantly larger than those of earthworm burrows at SZ. Figure 5 indicates that the combination of the high-resolution 3D laser scanning technology and the in-situ burrow extraction method provides a fast and reliable method to quantitatively analyze and characterize soil macropore morphology.

3.3 Circularity (*C*) and tortuosity (τ) of earthworm burrows

C is an important indicator to describe the cross-sectional shape of earthworm burrows, which may help to further understand the influence of macropore shape on water infiltration. The closer *C* is to 1, the more circular the cross-section of the burrow. The *C* values for earthworm burrows at LY and SZ were 0.888 ± 0.043 and 0.907 ± 0.039 (Table 3), respectively. Thus, the cross-sections of the burrows formed by earthworms was almost circular (Wuest, 2001). Because the closer the cross-section of the earthworm burrow was to being a circle, the smaller the inner surface area of the burrow walls, and the smaller the resistance to water flow. The *C* values of the earthworm burrows were negatively correlated with *A* and *D* values (Table 4) (Lebron, Suarez & Schaap, 2002). This result was consistent with the findings of (Li, Shao & Jia, 2016), who demonstrated that the larger the cross-sectional area (or pore size) of soil macropore, the more irregular the shape. Larger burrows were more susceptible to collapse and

deform due to external forces. In addition, results show (Table 5) that there was no difference between the C values at the two sites. This might suggest that differences in soil texture and tillage practices had little effect on C values of earthworm burrows. Further study is needed to clarify how soil texture and tillage practices influence earthworm burrow morphology.

Table 3 shows that the τ values of earthworm burrows at LY and SZ were 1.143 ± 0.082 and 1.133 ± 0.108, respectively. Statistically, these two τ values were not significantly different from each other (Table 5). This indicated that for megascolecidae, the value of τ did not vary among different locations under different farming treatments. The almost universal value of τ is of great value for simulating water and solute transport in macropores, because the whole simulation process can be significantly simplified by using τ with a constant value. In order to verify the above conclusions, more studies on the extraction of spatial morphological features of burrows of anecic earthworms in different soils are needed in the future. Based on CT scanning and image processing, Zhang et al. (2018) calculated τ values of biological pores in farm soil to be 1.243 ± 0.013, Luo, Lin and Li (2010) calculated the τ values of macropores in farm land soil to be 1.332, which were both larger than our results. The reason that their τ values differed from our values could be due to subjective image segmentation thresholds of CT scanning. Another possible explanation could be that the soil column studied by Luo, Lin and Li (2010) included not only earthworm pores, but also complex pores formed by plant roots, freeze-thaw alternations, and dry-wet alternations, which could result in larger calculated τ values. Unlike the method of Luo, Lin and Li (2010), our method only included the spatial parameters of earthworm burrows.

3.4 Diameter (*D*) and cross-sectional area (*A*) of earthworm burrows

There were significant differences in *D* and *A* of earthworm burrows between the two test sites (Table 5), *D* (6.456 ± 1.58 mm) and *A* (36.929 ± 21.656 mm^2) of earthworm burrows at LY were 1.8 times and 3.4 times larger than *D* (3.449 ± 0.531 mm) and *A* (9.786 ± 2.885 mm^2) at SZ. The different tillage methods at the two sites could affect the species composition and diversity of earthworms directly (Chan, 2001), while different species of earthworms could form burrows of different aperture sizes through burrowing activities. Rotary tillage could cause significant reductions in large earthworms through mechanical damage, while the relatively small earthworms were able to better survive. Our genetic sequencing of earthworms from the two test sites showed that the no-till (LY) was dominated by large and thick Metaphire vulgaris, while rotary tillage (SZ) was dominated by medium-sized and thin Amynthas amis. The results indirectly verified the analysis of variance (ANOVA) of *D* and *A* (Table 5). Other factors that could cause significant differences in *D* and *A* of earthworm burrows at the two test sites included: (1) The loss of nutrients from the soil surface at SZ caused the soil organic matter content to be greatly reduced, which further reduced the growth and reproduction of large adult earthworms. (2) The external compacting pressure caused by mechanical rotary tillage relocated soil inwards reducing the *D* and *A* of burrows (Schrader, Rogasik, Onasch & Jégou, 2007). (3) The larger sand content of soil at SZ weakened the structural strength of the soil, making it difficult to form larger earthworm burrows.

4 CONCLUSION

Macropore geometry is essential when modeling non-equilibrium flow and transport. The

approach proposed in this study allows for detailed characterizations of the spatial morphology features of anecic earthworm burrows. The results showed that metal tin could be applied to determine the surface opening of earthworm burrow structures. The spatial structure of earthworm burrows (cross-sectional area (A), circularity (C), diameter (D), actual length (L_t) and tortuosity (τ)) could be accurately obtained for the excavated earthworm burrow casts with a 3D laser scanner. The results showed that the earthworm burrows cross-sections were nearly circular. Statistically, the differences in τ values of earthworm burrows between the two different test sites were not significant. Our results also implied that different tillage methods, soil texture and soil organic matter content might affect cross-sectional area (A) and the diameter (D) of earthworm burrows. The tin casting method improved our understanding of macropore structure of soil animals, although the method was limited to burrows open at the soil surface. In addition, the tin casting method was not suitable for saturated and nearly saturated soils. Additional future research is needed to separate the influence of soil types and tillage methods on the spatial morphology of earthworm burrows.

ACKNOWLEDGEMENTS

This work was supported by Natural Science Foundation of China Grant No 42077008, Grant No 41771257, and USDA-NIFA Multi-State Project 4188.

AUTHOR CONTRIBUTIONS

Na Wen: Conceptualization; Investigation; Methodology; Software; Visualization; Writing-original draft; Data curation. Jie Zhang: Formal analysis; Resources; Supervision. Hui Zeng: Formal analysis; Resources; Supervision. Gang Liu: Conceptualization; Funding

acquisition; Investigation; Methodology; Project administration; Resources; Software; Supervision; Validation; Writing-review & editing. Robert Horton: Funding acquisition; Supervision; Writing-review & editing.

CONFLICT OF INTEREST

We declare that there is no conflict of interest in connection with the work submitted.

References:

Abou Najm, M. R., Jabro, J. D., Iversen, W. M., Mohtar, R. H., & Evans, R. G. (2010). New method for the characterization of three-dimensional preferential flow paths in the field. *Water Resources Research*, 46, http://dx.doi.org/10.1029/2009WR008594

Alavi, S., & Passandideh-Fard, M. (2011). Numerical simulation of droplet impact and solidification including thermal shrinkage in a thermal spray process. *Frontiers in Heat and Mass Transfer*, 2, http://dx.doi.org/10.5098/hmt.v2.2.3007

Bastardie, F., Capowiez, Y., de Dreuzy, J. R., & Cluzeau, D. (2003). X-ray tomographic and hydraulic characterization of burrowing by three earthworm species in repacked soil cores. *Applied Soil Ecology*, 24, 3-16. http://dx.doi.org/10.1016/S0929-1393(03)00071-4

Borges, J. A. R., Pires, L. F., Cássaro, F. A. M., Auler, A. C., Rosa, J. A., Heck, R. J., ... Roque, W. L. (2019). X-ray computed tomography for assessing the effect of tillage systems on topsoil morphological attributes. *Soil and Tillage Research*, 189, 25-35. http://dx.doi.org/10.1016/j.still.2018.12.019

Capowiez, Y., Bottinelli, N., Sammartino, S., Michel, E., & Jouquet, P. (2015). Morphological and functional characterisation of the burrow systems of six earthworm species (Lumbricidae). *Biology and Fertility of Soils*, 51, 869-877. http://dx.doi.org/10.1007/s00374-015-1036-x

Capowiez, Y., Sammartino, S., & Michel, E. (2011). Using X-ray tomography to quantify earthworm bioturbation non-destructively in repacked soil cores. *Geoderma*, 162, 124-131. http://dx.doi.org/10.1016/j.geoderma.2011.01.011

Cercioglu, M. (2018). Imaging soil pore characteristics using computed tomography as influenced by agroecosystems. *Eurasian Journal of Soil Science*, 7, http://dx.doi.org/10.18393/ejss.396237

Chan, K. Y. (2001). An overview of some tillage impacts on earthworm population abundance and diversity - implications for functioning in soils. *Soil & Tillage Research*, 57, 179-191. http://dx.doi.org/10.1016/S0167-1987(00)00173-2

Filipović, V., Defterdarović, J., Šimůnek, J., Filipović, L., Ondrašek, G., Romić, D., ... Kodešová, R. (2020). Estimation of vineyard soil structure and preferential flow using dye

tracer, X-ray tomography, and numerical simulations. *Geoderma*, 380, 114699. http://dx.doi.org/10.1016/j.geoderma.2020.114699

Gancarz, T., Moser, Z., Gąsior, W., Pstruś, J., & Henein, H. (2011). A comparison of surface tension, viscosity, and density of sn and sn–ag alloys using different measurement techniques. *International Journal of Thermophysics*, 32, 1210-1233. http://dx.doi.org/10.1007/s10765-011-1011-1

Gavinelli, F., Barcaro, T., Csuzdi, C., Blakemore, R. J., Fernandez Marchan, D., De Sosa, I., ... Paoletti, M. G. (2018). Importance of large, deep-burrowing and anecic earthworms in forested and cultivated areas (vineyards) of northeastern Italy. *Applied Soil Ecology*, 123, 751-774. http://dx.doi.org/10.1016/j.apsoil.2017.07.012

Gebrenegus, T., Ghezzehei, T. A., & Tuller, M. (2011). Physicochemical controls on initiation and evolution of desiccation cracks in sand-bentonite mixtures: X-ray CT imaging and stochastic modeling. *Journal of Contaminant Hydrology*, 126, 100-112. http://dx.doi.org/10.1016/j.jconhyd.2011.07.004

Germán-Heins, J., & Flury, M. (2000). Sorption of Brilliant Blue FCF in soils as affected by pH and ionic strength. *Geoderma*, 97, 87-101. http://dx.doi.org/https://doi.org/10.1016/S0016-7061(00)00027-6

Hanna, H. M., Steward, B. L., & Aldinger, L. (2010). Soil loading effects of planter Depth-Gauge wheels on early corn growth. *Applied Engineering in Agriculture*, 26, 551-556. http://dx.doi.org/10.13031/2013.32058

Iassonov, P., Gebrenegus, T., & Tuller, M. (2009). Segmentation of X-ray computed tomography images of porous materials: A crucial step for characterization and quantitative analysis of pore structures. *Water Resources Research*, 45, http://dx.doi.org/10.1029/2009WR008087

Kodešová, R., Němeček, K., Žigová, A., Nikodem, A., & Fér, M. (2015). Using dye tracer for visualizing roots impact on soil structure and soil porous system. *Biologia*, 70, 1439-1443. http://dx.doi.org/10.1515/biolog-2015-0166

Krisnanto, S., Rahardjo, H., Fredlund, D. G., & Leong, E. C. (2016). Water content of soil matrix during lateral water flow through cracked soil. *Engineering Geology*, 210, 168-179. http://dx.doi.org/10.1016/j.enggeo.2016.06.012

Kuzminsky, S. C., & Gardiner, M. S. (2012). Three-dimensional laser scanning: Potential uses for museum conservation and scientific research. *Journal of Archaeological Science*, 39, 2744-2751. http://dx.doi.org/10.1016/j.jas.2012.04.020

Le Mer, G., Jouquet, P., Capowiez, Y., Maeght, J., Tran, T. M., Doan, T. T., ... Bottinelli, N. (2021). Age matters: Dynamics of earthworm casts and burrows produced by the anecic Amynthas khami and their effects on soil water infiltration. *Geoderma*, 382, 114709. http://dx.doi.org/10.1016/j.geoderma.2020.114709

Lebron, I., Suarez, D. L., & Schaap, M. G. (2002). Soil pore size and geometry as a result of aggregate-size distribution and chemical composition. *Soil Science*, 167, 165-172. http://dx.doi.org/10.1097/00010694-200203000-00001

Li, T. C., Shao, M. A., Jia, Y. H., Jia, X. X., Huang, L. M., ... Gan, M. (2019). Small-scale observation on the effects of burrowing activities of ants on soil hydraulic processes. *European Journal of Soil Science*, 70, 236-244. http://dx.doi.org/10.1111/ejss.12748

Li, T. C., Shao, M. A., Jia, Y. H., Jia, X. X., & Huang, L. M. (2018). Small-scale observation on the effects of the burrowing activities of mole crickets on soil erosion and hydrologic processes. *Agriculture, Ecosystems & Environment*, 261, 136-143. http://dx.doi.org/10.1016/j.agee.2018.04.010

Li, T. C., Shao, M. A., & Jia, Y. H. (2016). Application of X-ray tomography to quantify macropore characteristics of loess soil under two perennial plants. *European Journal of Soil Science*, 67, 266-275. http://dx.doi.org/10.1111/ejss.12330

Li, T., Shao, M., Jia, Y., Jia, X., & Huang, L. (2018). Using the X-ray computed tomography method to predict the saturated hydraulic conductivity of the upper root zone in the Loess Plateau in China. *Soil Science Society of America Journal*, 82, 1085-1092. http://dx.doi.org/10.2136/sssaj2017.08.0268

Liang, H., Hu, K. L., Batchelor, W. D., Qi, Z. M., & Li, B. G. (2016). An integrated soil-crop system model for water and nitrogen management in North China. *Scientific Reports*, 6, http://dx.doi.org/10.1038/srep25755

Luo, L., Lin, H., & Li, S. (2010). Quantification of 3-D soil macropore networks in different soil types and land uses using computed tomography. *Journal of Hydrology*, 393, 53-64. http://dx.doi.org/10.1016/j.jhydrol.2010.03.031

Mooney, S. J. (2002). Three-dimensional visualization and quantification of soil macroporosity and water flow patterns using computed tomography. *Soil Use and Management*, 18, 142-151. http://dx.doi.org/10.1079/SUM2002121

Nawab, Y., Boyard, N., Sobotka, V., Casari, P., & Jacquemin, F. (2011). A device to measure the shrinkage and heat transfers during the curing cycle of thermoset composites. *Advanced Materials Research*, 326, 19-28. http://dx.doi.org/10.4028/www.scientific.net/AMR.326.19

Ni, X. M., Miao, J., Lv, R. S., & Lin, X. Y. (2017). Quantitative 3D spatial characterization and flow simulation of coal macropores based on μCT technology. *Fuel (Guildford)*, 200, 199-207. http://dx.doi.org/10.1016/j.fuel.2017.03.068

Pagenkemper, S. K., Athmann, M., Uteau, D., Kautz, T., Peth, S., ... Horn, R. (2015). The effect of earthworm activity on soil bioporosity – Investigated with X-ray computed tomography and endoscopy. *Soil and Tillage Research*, 146, 79-88. http://dx.doi.org/10.1016/j.still.2014.05.007

Peigne, J., Cannavaciuolo, M., Gautronneau, Y., Aveline, A., Giteau, J. L., ... Cluzeau, D. (2009). Earthworm populations under different tillage systems in organic farming. *Soil & Tillage Research*, 104, 207-214. http://dx.doi.org/10.1016/j.still.2009.02.011

Peleg, N., & Gvirtzman, H. (2010). Groundwater flow modeling of two-levels perched karstic leaking aquifers as a tool for estimating recharge and hydraulic parameters. *Journal of Hydrology*, 388, 13-27. http://dx.doi.org/10.1016/j.jhydrol.2010.04.015

Pelosi, C., Baudry, E., & Schmidt, O. (2021). Comparison of the mustard oil and electrical methods for sampling earthworm communities in rural and urban soils. *Urban Ecosystems*, 24, 355-364. http://dx.doi.org/10.1007/s11252-020-01023-0

Perret, J., Prasher, S. O., Kantzas, A., & Langford, C. (2000). A two-domain approach using CAT scanning to model solute transport in soil. *Journal of Environmental Quality*, 29, 995-1010. http://dx.doi.org/10.2134/jeq2000.00472425002900030039x

Peth, S., Horn, R., Beckmann, F., Donath, T., Fischer, J., ... Smucker, A. J. M. (2008). Three-dimensional quantification of intra-aggregate pore-space features using synchrotron-radiation-based microtomography. *Soil Science Society of America Journal*, 72, 897-907. http://dx.doi.org/10.2136/sssaj2007.0130

Reis, J. M. L. D. (2012). Effect of temperature on the mechanical properties of polymer mortars. *Materials Research*, 15, 645-649. http://dx.doi.org/10.1590/S1516-14392012005000091

Rossi, A. M., Hirmas, D. R., Graham, R. C., & Sternberg, P. D. (2008). Bulk density determination by automated Three-Dimensional laser scanning. *Soil Science Society of America Journal*, 72, 1591-1593. http://dx.doi.org/10.2136/sssaj2008.0072N

Schrader, S., Rogasik, H., Onasch, I., & Jégou, D. (2007). Assessment of soil structural differentiation around earthworm burrows by means of X-ray computed tomography and scanning electron microscopy. *Geoderma*, 137, 378-387. http://dx.doi.org/10.1016/j.geoderma.2006.08.030

Šimůnek, J., van Genuchten, M. T., & Šejna, M. (2008). Development and applications of the HYDRUS and STANMOD software packages and related codes. *Vadose Zone Journal*, 7, 587-600. http://dx.doi.org/10.2136/vzj2007.0077

Taina, I. A., Heck, R. J., & Elliot, T. R. (2008). Application of X-ray computed tomography to soil science: A literature review. *Canadian Journal of Soil Science*, 88, 1-20. http://dx.doi.org/10.4141/CJSS06027

Takacs, V., Molnar, L., Klimek, B., Galuszka, A., Morgan, A. J., ... Plytycz, B. (2016). Exposure of Eisenia andrei (Oligochaeta; Lumbricidea) to Cadmium Polluted Soil Inhibits Earthworm Maturation and Reproduction but not Restoration of Experimentally Depleted Coelomocytes or Regeneration of Amputated Segments. *Folia Biologica-Krakow*, 64, 275-284. http://dx.doi.org/10.3409/fb64_4.275

Tippkoetter, R., & Ritz, K. (1996). Evaluation of polyester, epoxy and acrylic resins for suitability in preparation of soil thin sections for in situ biological studies. *Geoderma*, 69, 31-57. http://dx.doi.org/10.1016/0016-7061(95)00041-0

Wuest, S. B. (2001). Soil biopore estimation: Effects of tillage, nitrogen, and photographic resolution. *Soil & Tillage Research*, 62, 111-116. http://dx.doi.org/10.1016/S0167-1987(01)00218-5

Zhang, C., Wu, D., Tong, X., Zhu, Y., Xu, S., Xiong, D., ... Chu, P. K. (2017). Highly efficient field emission from ZnO nanorods and nanographene hybrids on a macroporous electric conductive network. *Journal of Materials Chemistry C*, 5, 9296-9305.

http://dx.doi.org/10.1039/c7tc02821k

Zhang, J., Lei, T., Qu, L., Zhang, M., Chen, P., Gao, X., ... Yuan, L. (2019). Method to quantitatively partition the temporal preferential flow and matrix infiltration in forest soil. *Geoderma*, 347, 150-159. http://dx.doi.org/10.1016/j.geoderma.2019.03.026

Zhang, J., Lei, T., & Chen, T. (2016). Impact of preferential and lateral flows of water on Single-Ring measured infiltration process and its analysis. *Soil Science Society of America Journal*, 80, 859-869. http://dx.doi.org/10.2136/sssaj2015.12.0445

Zhang, Z., Liu, K., Zhou, H., Lin, H., Li, D., ... Peng, X. (2018). Three dimensional characteristics of biopores and non-biopores in the subsoil respond differently to land use and fertilization. *Plant and Soil*, 428, 453-467. http://dx.doi.org/10.1007/s11104-018-3689-3

FIGURE CAPTIONS

FIGURE 1 Schematic diagram of the geographic location of two study sites.

FIGURE 2 (a) A field research area. (b) 1 m^2 divided plot and flags for marking the earthworm burrows. (c) The yellow oval indicates earthworm feces. (d) Solidified tin castings.

FIGURE 3 Schematic diagram of the 3D laser scanner, the tin casting of one earthworm burrow, software interface for the 3D laser scanner and the digitalized three-dimensional earthworm burrow profile.

FIGURE 4 The three-dimensional spatial geometry structure diagram of one earthworm burrow and the definition of model parameter L_l and L_t (tin casting # LY-1 as an example).

FIGURE 5 Three-dimensional earthworm burrow spatial structures reconstructed by a 3D laser scanner.

526 **FIGURE 1** Schematic diagram of the geographic location of two study sites.

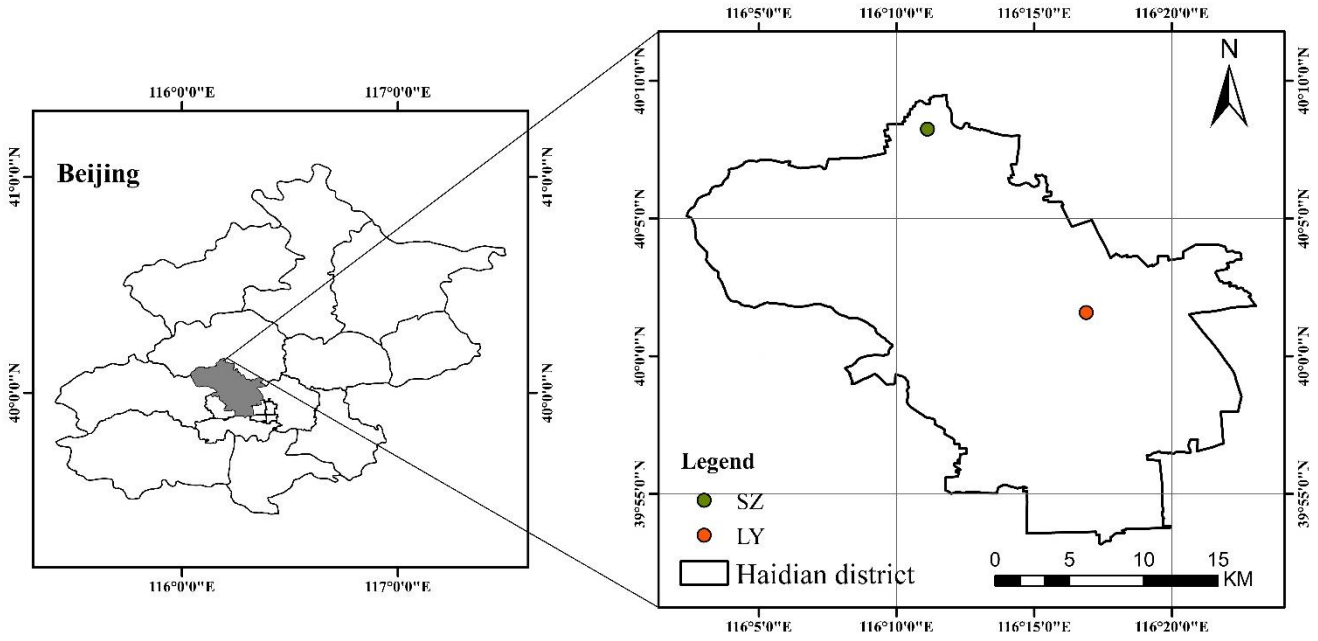

FIGURE 2 (a) A field research area. (b) 1 m^2 divided plot and flags for marking the earthworm burrows. (c) The yellow oval indicates earthworm feces. (d) Solidified tin castings.

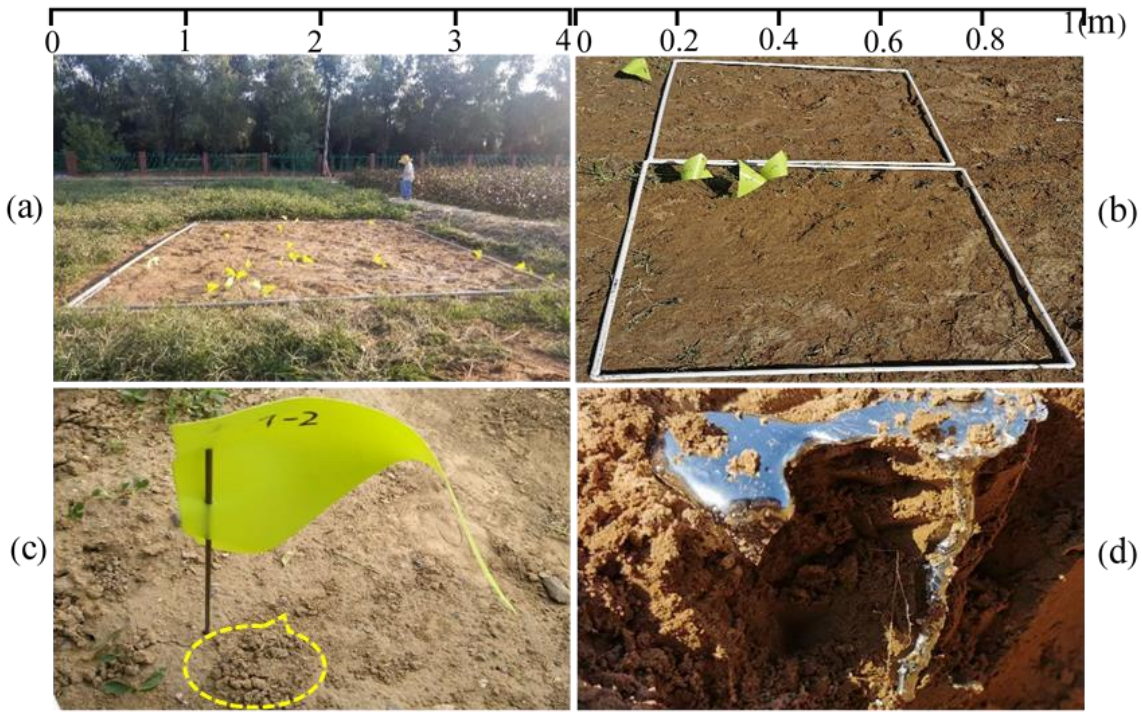

FIGURE 3 Schematic diagram of the 3D laser scanner, the tin casting of one earthworm burrow, software interface for the 3D laser scanner and the digitalized three-dimensional earthworm burrow profile.

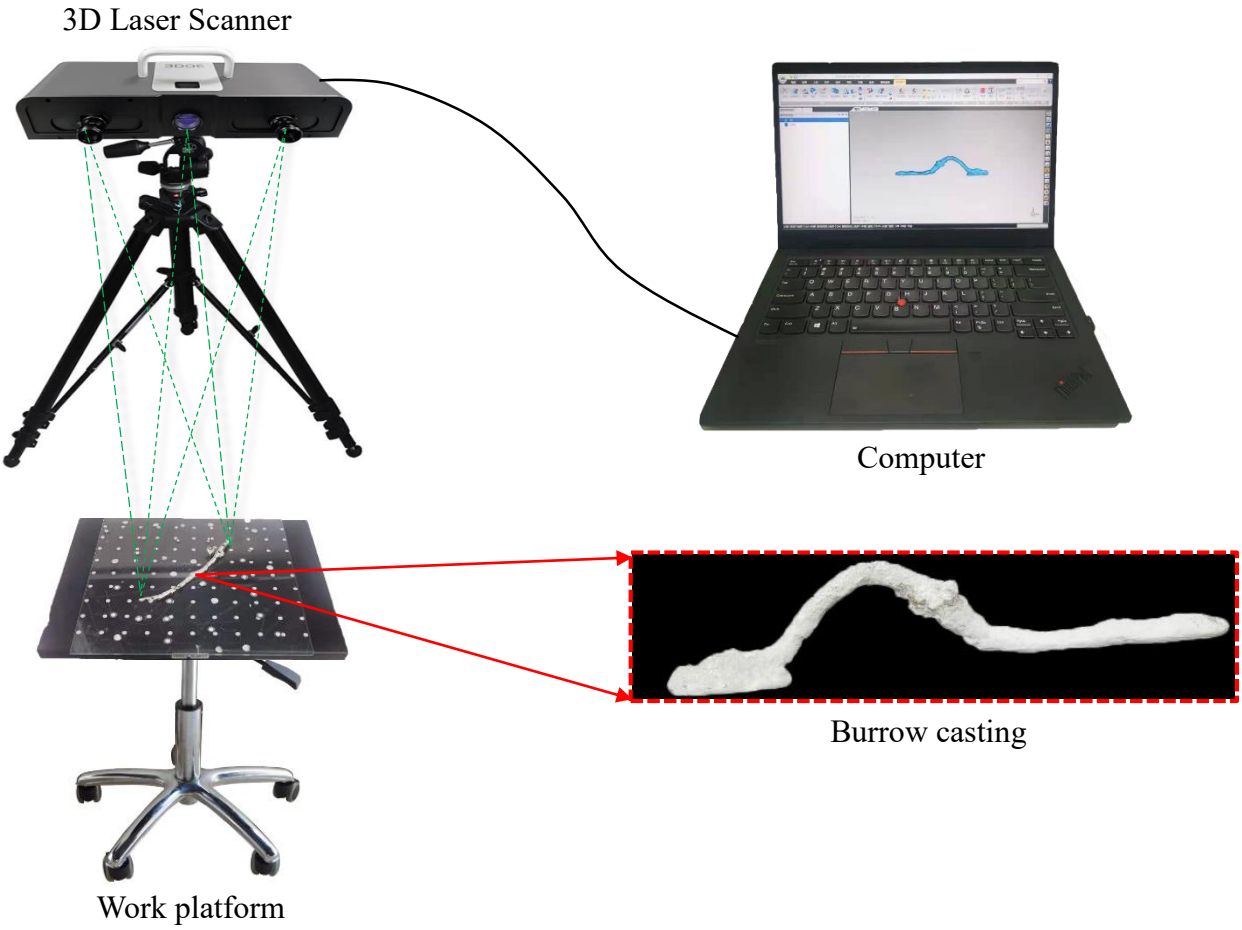

FIGURE 4 The three-dimensional spatial geometry structure diagram of one earthworm burrow and the definition of model parameter L_1 and L_t (tin casting # LY-1 as an example).

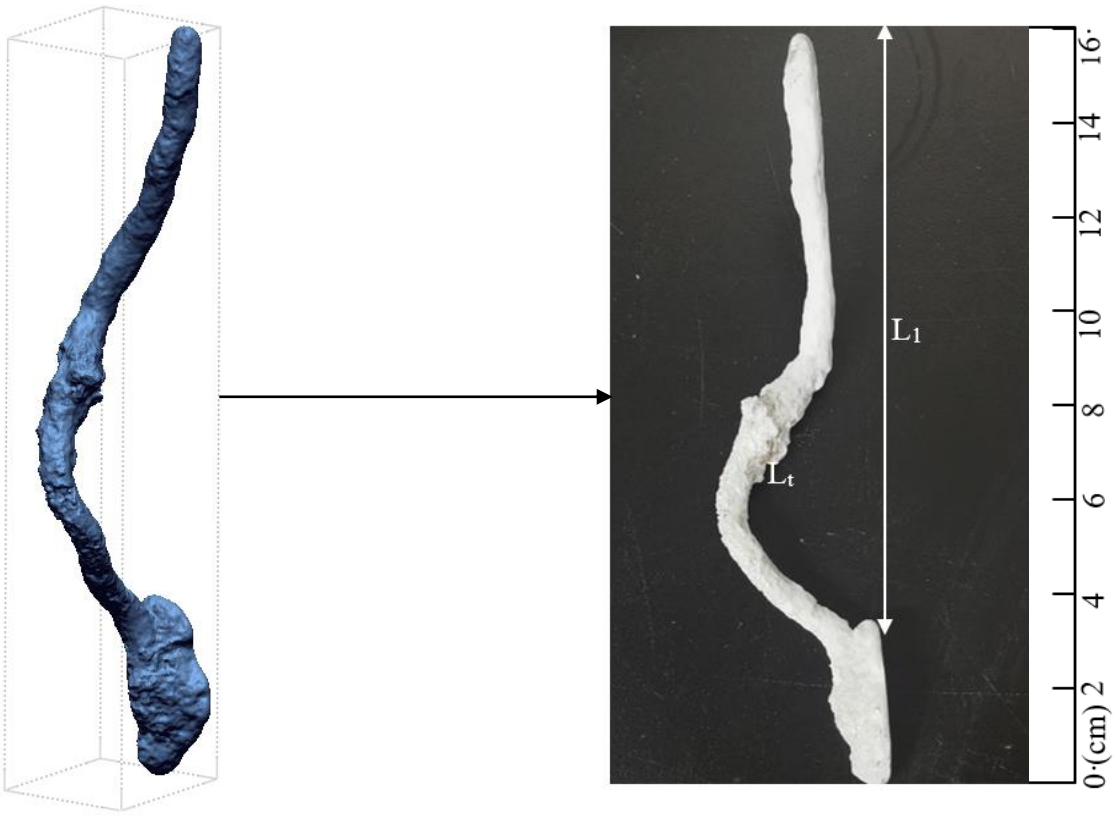

534 **FIGURE 5** Three-dimensional earthworm burrow spatial structures reconstructed by a 3D laser

535 scanner.

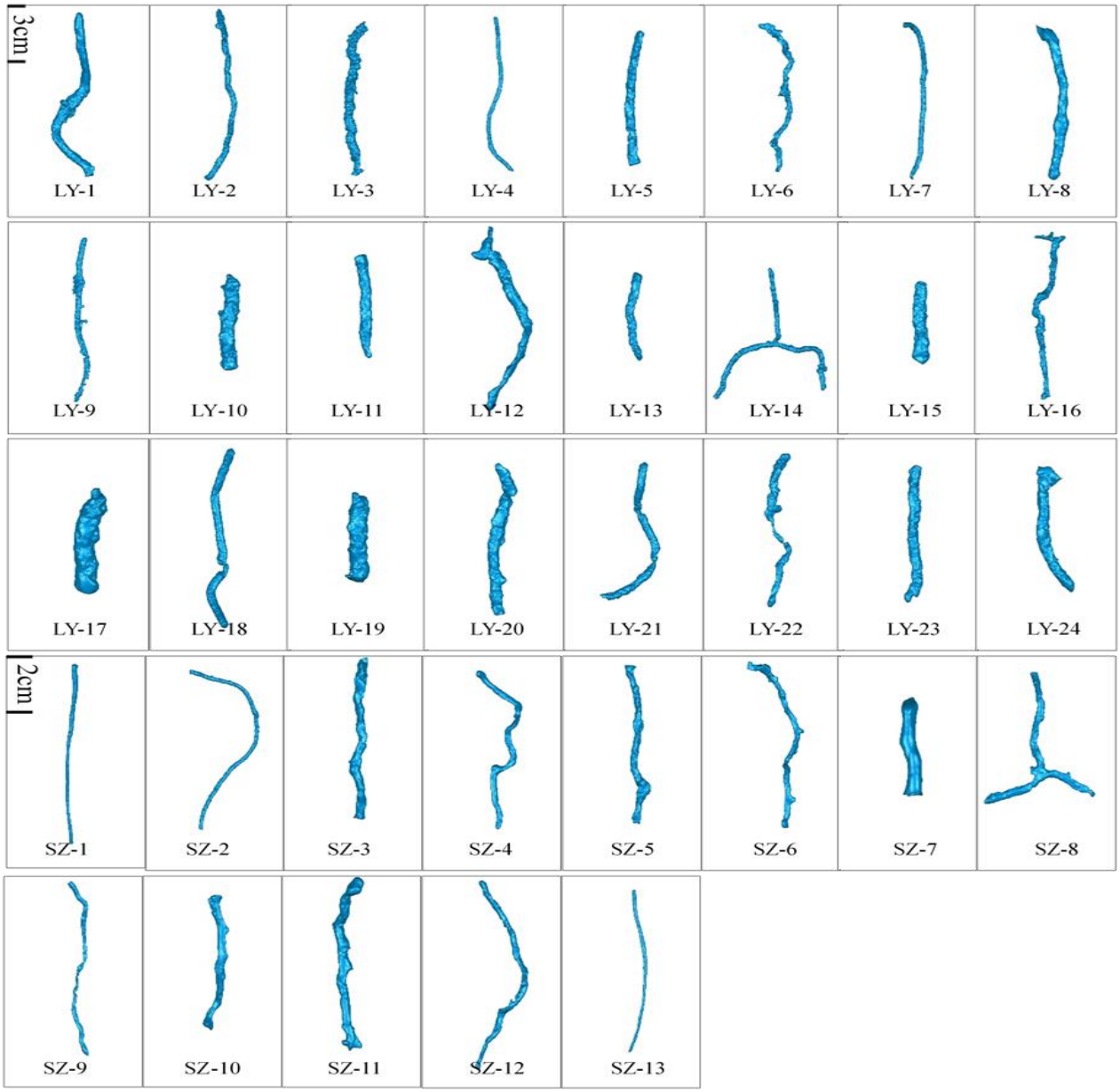

TABLE 1 Earthworm species of LY and SZ obtained by gene sequencing. († stands for the accession number from the website of NCBI for earthworm genome classification. ‡ At each site, a total of 20 earthworms were selected for gene sequence analysis, this column listed the number of successfully sequenced samples. Earthworm species were classified according to References: 1 (Fang, 2021), 2 (Shen, 2012) and 3 (Teng, 2013)).

Site	Family	Genus	Species	Accession number †	Number of samples ‡
LY	Megascolex	Metaphire	Metaphire vulgaris [1]	KJ137279	16
SZ	Megascolex	Amynthas	Amynthas amis [2]	KP030700	9
SZ	Megascolex	Metaphire	Metaphire vulgaris [1]	KJ137279	2
SZ	Megascolex	Metaphire	Metaphire tschiliensis tschiliensis [3]	DQ835677	3

TABLE 2 Abundance of earthworms and burrows, and total number of castings extracted at each site.

Site	Earthworm population density (individuals / m^2)	Burrows density (burrows / m^2)	Number of castings
LY	16.1	2.7	28/24
SZ	4.2	1.4	17/13

Note: 28/24 represents 28 earthworm burrow castings were extracted from the LY site, and 24 burrow castings were digitally swept; 17/13 represents 17 earthworm burrow castings were extracted from the SZ site, and 13 burrow castings were digitally swept.

546 **TABLE 3** Characteristic parameters of earthworm burrows at two sites (±represents standard

547 deviation).

	LY	SZ
	Mean Value	Mean Value
D (mm)	6.456±1.585	3.449±0.531
A (mm^2)	36.929±21.656	9.786±2.885
L_t (mm)	139.526±70.421	105.852±52.848
τ	1.143±0.082	1.133±0.108
C	0.888±0.043	0.907±0.039

548 **TABLE 4** Pearson correlation coefficient among different earthworm burrows geometry

549 characteristics.

	A (mm^2)	D (mm)	C	L_t (mm)
D (mm)	0.941 (0.000**)			
C	-0.515 (0.001**)	-0.471 (0.003**)		
L_t (mm)	0.349 (0.016*)	0.368 (0.025*)	-0.048 (0.777)	
τ	0.058 (0.734)	0.045 (0.793)	-0.191 (0.258)	0.064 (0.707)

550 Note: Probability value in parentheses are indicated by two significance levels (**< 0.01, *<0.05).

TABLE 5 Analysis of variance of the spatial characteristic parameters of earthworm burrows at two experimental sites.

Variable	F	Significance
D (mm)	43.505	0.000**
A (mm^2)	19.957	0.000**
L_t (mm)	2.268	0.141
τ	0.109	0.743
C	1.622	0.211

Note: Values of p are indicated using two significance levels (**< 0.01, *<0.05).